Electronic structure of $Fe_{1.04}Te_{0.66}Se_{0.34}$

Fei Chen,[1] Bo Zhou,[1] Yan Zhang,[1] Jia Wei,[1] Hong-Wei Ou,[1] Jia-Feng Zhao,[1] Cheng He,[1] Qing-Qin Ge,[1] Masashi Arita,[2] Kenya Shimada,[2] Hirofumi Namatame,[2] Masaki Taniguchi,[2] Zhong-Yi Lu,[3] Jiangping Hu,[4] Xiao-Yu Cui,[5] and D. L. Feng[1,*]

[1]*Department of Physics, Surface Physics Laboratory (National Key Laboratory), and Advanced Materials Laboratory, Fudan University, Shanghai 200433, People's Republic of China*

[2]*Hiroshima Synchrotron Radiation Center and Graduate School of Science, Hiroshima University, Hiroshima 739-8526, Japan*

[3]*Department of Physics, Renmin University of China, Beijing 100872, People's Republic of China*

[4]*Department of Physics, Purdue University, West Lafayette, Indiana 47907, USA*

[5]*Swiss Light Source, Paul-Scherrer Institut, 5232 Villigen, Switzerland*

(Received 15 November 2009; revised manuscript received 2 January 2010; published 28 January 2010)

We report the electronic structure of the iron-chalcogenide superconductor, $Fe_{1.04}(Te_{0.66}Se_{0.34})$, obtained with high-resolution angle-resolved photoemission spectroscopy and density-functional calculations. In photoemission measurements, various photon energies and polarizations are exploited to study the Fermi surface topology and symmetry properties of the bands. The measured band structure and their symmetry characters qualitatively agree with our density-functional theory calculations of $Fe(Te_{0.66}Se_{0.34})$, although the band structure is renormalized by about a factor of three. We find that the electronic structures of this iron chalcogenides and the iron pnictides have many aspects in common; however, significant differences exist near the Γ point. For $Fe_{1.04}Te_{0.66}Se_{0.34}$, there are clearly separated three bands with distinct even or odd symmetry that cross the Fermi energy (E_F) near the zone center, which contribute to three holelike Fermi surfaces. Especially, both experiments and calculations show a holelike elliptical Fermi surface at the zone center. Moreover, no sign of spin density wave was observed in the electronic structure and susceptibility measurements of this compound.

DOI: 10.1103/PhysRevB.81.014526 PACS number(s): 74.25.Jb, 74.70.−b, 79.60.−i, 71.20.−b

I. INTRODUCTION

The discovery of superconductivity with the superconducting transition temperature (T_c) up to 55 K in iron pnictides[1–3] has generated great interests. The FeAs layer is considered as the key structure for superconductivity in systems ranging from $SmO_{1-x}F_xFeAs$ and $Ba_{1-x}K_xFe_2As_2$,[4,5] to LiFeAs.[6,7] Recently, certain iron chalcogenides, e.g., $Fe_{1+x}Se$ and $Fe_{1+y}Te_{1-x}Se_x$,[8,9] have been found to be superconducting as well. $Fe_{1+x}Se$ shows superconductivity at 8 K under ambient pressure[8] and 37 K under a 7 GPa hydrostatic pressure,[10] which is comparable to $Ba_{1-x}K_xFe_2As_2$ (T_c =38 K).[5] Because iron chalcogenides do not involve arsenic, it would be particularly important for applications. Furthermore, although Fe 3*d* orbitals play a vital role in the iron-based high-temperature superconductors, the anions seem also play an important role on various aspects, noting LaOFeP possesses a T_c of merely 5 K. Besides the size effect, the polarizability of the anions has even been suggested to be crucial for the superconductivity.[11] Therefore, iron chalcogenides provide an opportunity to study the role of anions in iron-based superconductors.

The iron pnictides and iron chalcogenides have many things in common. The FeSe(Te) layer in $Fe_{1+y}Te_{1-x}Se_x$ is isostructural to the FeAs or FeP layer in iron pnictides. Moreover, the phase diagram of $Fe_{1+y}Te_{1-x}Se_x$ resembles that of the iron pnictides, where the competition between magnetism and superconductivity has been observed in both cases. The undoped $Fe_{1+y}Te$ exhibits a spin density wave (SDW) ground state. With sufficient selenium doping, the SDW is suppressed, and the superconductivity occurs at a T_c as high as 15 K.[9]

There are also critical differences between the iron pnictides and iron chalcogenides, in particular, between their structures of magnetic ordering. A common collinear commensurate antiferromagnetic (AFM) ordering has been identified in all iron pnictides. However, the magnetic state of the $Fe_{1+y}Te_{1-x}Se_x$ family has a bicollinear commensurate or incommensurate antiferromagnetic ordering depending on the concentration of the interstitial iron.[12,13] It is still in a heated debate about the origin of magnetic ordering in iron-based superconductors. While models based on local moments have been suggested to understand both magnetic orderings,[14–19] the collinear AFM in the iron pnictides in principle can originate from nesting mechanism between the hole pockets at Γ and the electron pockets at *M*,[20] but the bicollinear magnetic structure is inconsistent with this picture since there is no Fermi surface at *X*. Is there a connection between the electronic structure and magnetic ordering in the iron chalcogenides? If there is, what is the connection? The answers of these fundamental questions require a deep understanding of the electronic structures of iron chalcogenides. However, there is just few data reported on the electronic structure of iron chalcogenides.[21]

In this paper, we investigate the electronic structure of $Fe_{1.04}Te_{0.66}Se_{0.34}$ with high-resolution angle-resolved photoemission spectroscopy (ARPES) and band calculation. The measured Fermi surfaces and the band structure are identified and found to qualitatively agree with the density-functional theory (DFT) calculations. The orbital characters of individual bands are studied by polarization dependence studies and found to agree with the calculation as well. No obvious effect of the fluctuating SDW is observed on the electronic structure. Furthermore, we found that although most aspects of the electronic structure of this iron chalcogenide are simi-

lar to the iron pnictides, there are clearly three separated bands at the zone center for the iron chalcogenides, while there appear just two separated features for the normal state of iron pnictides. Moreover, the symmetry properties of the iron-chalcogenide bands near the zone center are different from those of the iron pnictides. The difference and similarity between the iron pnictides and iron chalcogenides in their electronic structure may shed light on our understanding of the role of anions and the superconductivity in iron-based superconductors.

II. MATERIAL AND EXPERIMENTAL SETUP

$Fe_{1.04}Te_{0.66}Se_{0.34}$ single crystal was synthesized with the NaCl/KCl-flux method. Fe powder, Te powder and Se powder were weighed according to the ratio of Fe:Te:Se =1:0.7:0.3 (mole) and pressed into thin plates. Then Fe-Te(Se) polycrystal was acquired by reacting the plate in an evacuated quartz tube at 1173 K for 24 h. FeTe(Se) polycrystal and the NaCl/KCl flux were weighed according to the ratio of FeTe(Se):NaCl/KCl=1:10 (mass). They were thoroughly grounded into a mixture and loaded into an evacuated quartz tube. The tube was kept at 1223 K for 24 h and then slowly cooled to 873 K in 100 h. Finally the quartz tube was cooled in the furnace after shutting off the power. $Fe_{1.04}Te_{0.66}Se_{0.34}$ single crystal was obtained after dissolving the flux in de-ionized water. The element compositions of this single crystal were determined through energy-dispersive x-ray (EDX) analysis with dense sampling spots across a 0.4×0.4 mm^2 surface area. The EDX result shows that the sample is homogeneous, and the maximal deviation of its compositions is within 1.8%. The temperature dependence of the magnetic susceptibility (Fig. 1) does not show any signs of SDW or structural transition. The resistivity data indicate that crystal reaches the zero resistance at about 9 K. However, the susceptibility measurements show that although regions of the sample become superconducting at 9 K, it reaches a bulk superconducting state at 2 K, with a transition width less than 3 K (10%–90%). This indicates that the bulk of the single crystal is quite homogeneous. With 1 T magnetic field, superconductivity is suppressed, and there is no sign of field-induced metamagnetic transition.

The photoemission data have been taken with Scienta R4000 electron analyzers at Beamline 9 of Hiroshima synchrotron radiation center (HSRC) and the surface and interface spectroscopy (SIS) beamline of Swiss light source (SLS). The typical angular resolution is 0.3° and the typical energy resolution is 15 meV. The sample was cleaved *in situ* and measured under ultrahigh vacuum better than 5×10^{-11} torr. The sample aging effects are carefully monitored to ensure they do not cause artifacts in our analyses and conclusions. The SIS beamline is equipped with an elliptically polarized undulator, which could switch the photon polarization between horizontal, vertical, or circular mode. This facilitates the polarization dependence studies, which is useful in determining the orbital characters of the bands.[22]

III. BAND STRUCTURE AND FERMI SURFACE

The photoemission intensities distribution of $Fe_{1.04}Te_{0.66}Se_{0.34}$ at the Fermi energy is shown in Fig. 2(a).

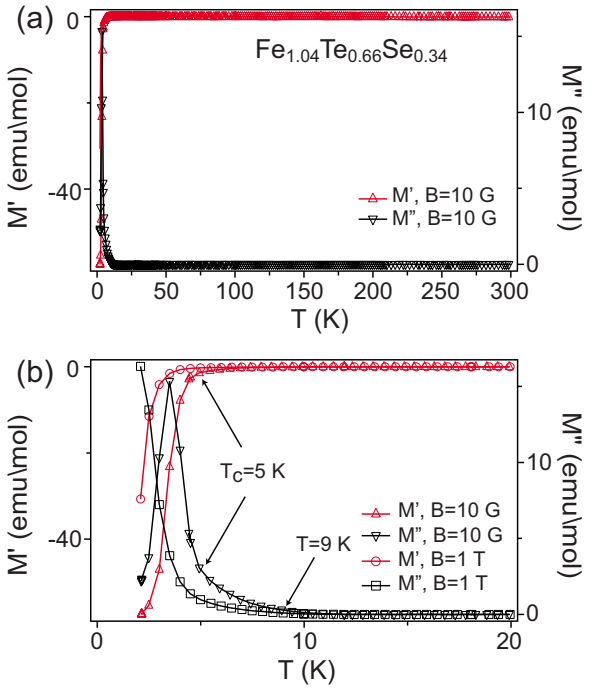

FIG. 1. (Color online) (a) Real and imaginary parts of the magnetic susceptibility of $Fe_{1.04}Te_{0.66}Se_{0.34}$ single crystal at 10 Gauss. The data were taken with the zero field cool (ZFC) procedure. (b) The low-temperature magnetic susceptibility data at 10 Gauss and 1 T magnetic field.

The data were taken at 15 K with 22 eV photons. Similar to the iron-pnictides, the spectral weight is mostly located around Γ and *M*. In order to resolve the details of the Fermi crossings, Fig. 2(c) shows the photoemission intensity along cut 1 in the Γ-*M* direction, several bands could be resolved. For a better visualization of the bands, Fig. 2(d) shows the second derivative with respect to energy for the data in Fig. 2(c). Three bands, α, β, and γ, could be clearly identified. The top of the α band is very close to the Fermi energy, but it is hard to judge whether it crosses E_F based on the energy distribution curves (EDCs) in Fig. 2(f). By judging from the momentum distribution curves (MDCs) in Fig. 2(g) near Γ, one finds that it crosses the Fermi level with a very small-sized Fermi surface. In order to check whether the spectral weight around *M* represents band crossings, the data in Fig. 2(c) is renormalized by its angular integrated spectrum and shown in Fig. 2(e). In this way, another band, δ, is resolved. The MDCs in the boxed region are shown in Fig. 2(h), where one observes an electron-pocket type of dispersion. This is similar to the $BaFe_2As_2$,[23] the δ band is quite weak in such an experimental geometry due to the strong orbital dependence of the matrix element.[22] Similarly, Figs. 2(i) and 2(j) show the photoemission intensity and its second derivative plot along the Γ-*X* direction, where α, β, and γ bands are observed. Therefore, there are totally three bands near the Γ point, and they all cross the Fermi surface and form three hole pockets. Based on the identified band dispersions, the Fermi crossings are determined and shown in Fig. 2(b). We note because of symmetry constraints, only crossings for one elliptical Fermi surface could be observed around *M* or *M'*.[22] The experimental Fermi surfaces are determined by fitting

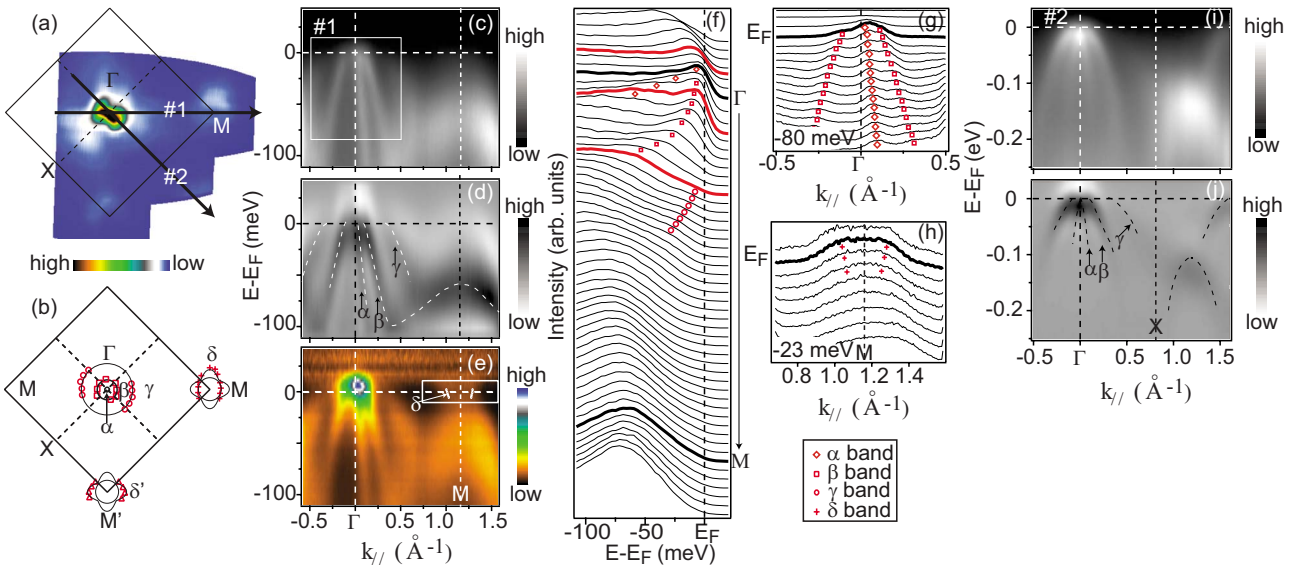

FIG. 2. (Color online) (a) Photoemission intensity distribution integrated over $[E_F-5$ meV, E_F+5 meV$]$ window for $Fe_{1.04}Te_{0.66}Se_{0.34}$. (b) The Fermi surfaces are constructed based on the measured Fermi crossings, which are labeled by squares, circles, crosses, and triangles for the β, γ, δ, and δ' bands respectively. (c) The photoemission intensity along the cut #1 in the Γ-M direction and (d) its second derivative with respect to energy. (e) The data in panel c is replotted after dividing the angle integrated energy distribution curve. (f) The EDCs for data in panel c. (g) The MDCs in the box area of panel c. (h) The MDCs in the box area of panel e. The crosses mark the feature positions based on a double Lorenzian fit. (i) The photoemission intensity along the cut #2 in the Γ-X direction, and (j) its second derivative. Data were taken with circularly polarized 22 eV photons at HSRC.

the Fermi crossings with symmetry in consideration. Assuming the β, γ, and δ Fermi surfaces to be cylindrical, one could estimate the electron concentration based on the Luttinger theorem. We obtained 0.08 holes per unit cell. This is not inconsistent with the chemical formula, considering variations in the Fermi surface volume caused by k_z dispersion of the band structure.

To further illustrate the behavior of the α band, Fig. 3 shows three nearby cuts taken with 22 eV photons. When approaching $(k_x=0,\ k_y=0)$, the α band disperses rather rapidly with its top in each cut moving toward E_F. Based on the peak positions in the MDCs [Fig. 3(j)], one could observe a Fermi crossing of the α band very close to $(k_x=0,\ k_y=0)$, giving a small holelike Fermi surface. However, this Fermi crossing is not observed at several other photon energies such as 50 and 100 eV (Fig. 4). Since these momentum cuts sample through $(k_x,k_y)=(0,0)$ at different k_z, the α Fermi surface is thus a closed pocket. Moreover, in Figs. 4(j)–4(l), the EDCs have been divided by the temperature-broadened Fermi-Dirac distribution, where both the α and β bands appear to be degenerate within the experimental resolution at 22 eV. Based on the calculations below, it suggests that this data cut should be very close to the zone center, Γ.

IV. ELECTRONIC BAND STRUCTURE CALCULATION

To understand the data, we have calculated the electronic band structure for $FeTe_{0.66}Se_{0.34}$. In the calculations the plane-wave basis method was used.[24] We adopted the generalized gradient approximation of Perdew-Burke-Ernzerhof[25] for the exchange-correlation potentials. The ultrasoft pseudopotentials[26] were used to model the electron-ion interactions. After the full convergence test, the kinetic-energy cutoff and the charge-density cutoff of the plane-wave basis were chosen to be 600 and 4800 eV, respectively. The Gauss-

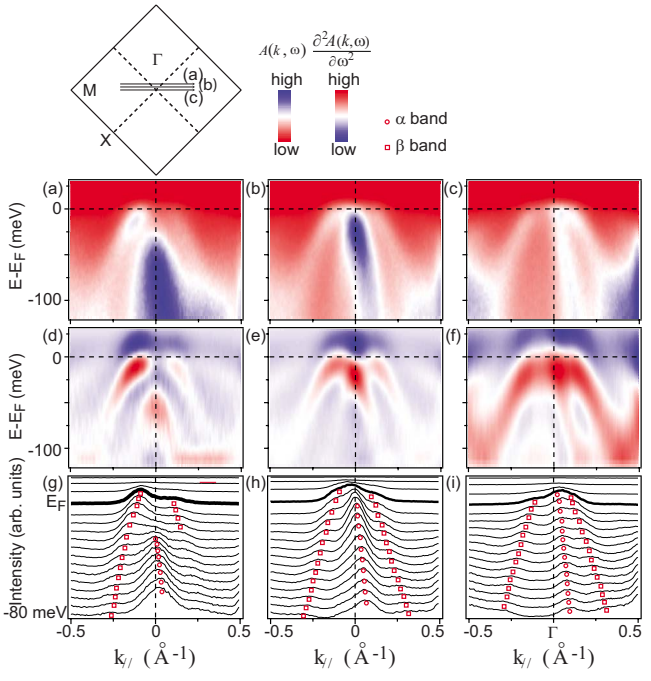

FIG. 3. (Color online) (a), (b), and (c) Photoemission data taken with 22 eV circularly polarized photons at HSRC along three momentum cuts as indicated in the Brillouin zone sketch. (d), (e), and (f) Second derivative with respect to energy for data in panels (a), (b), and (c), respectively. (g), (h), and (i) Momentum distribution curves near E_F for data in panels (a), (b), and (c), respectively.

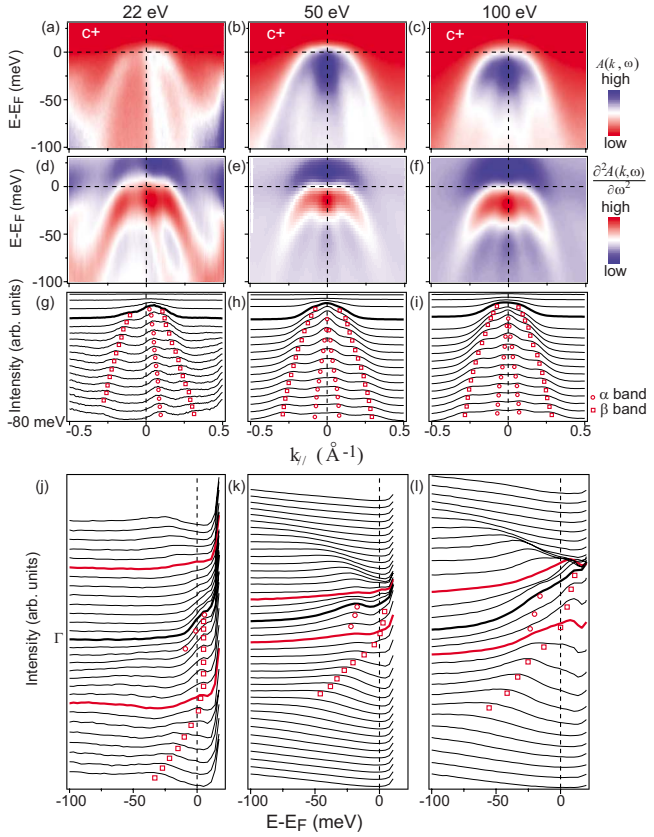

FIG. 4. (Color online) (a), (b), and (c) Photoemission data taken with 22 eV light at HSRC, and 50 and 100 eV circularly polarized light at SLS, respectively. All three momentum cuts cross the Γ-Z line (k_x=0, k_y=0,k_z) in the reciprocal space. (d), (e), and (f) Second derivative with respect to energy for data in panels (a), (b), and (c), respectively. (g), (h), and (i) Momentum distribution curves near E_F for data in panels (a), (b), and (c), respectively. (j), (k), and (l) Energy distribution curves for data in panels (a), (b), and (c), respectively, after divided by the Fermi-Dirac distribution function.

ian broadening technique was used and a mesh of 16×16 ×8 k points were sampled for the irreducible Brillouin zone integration. The internal atomic coordinates within a cell were determined by the energy minimization. The doping

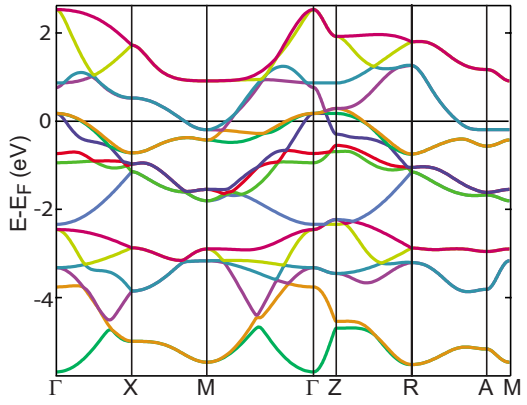

FIG. 5. (Color online) The calculated electronic band structure of $FeTe_{0.66}Se_{0.34}$ along high-symmetry lines in the irreducible Brillouin zone.

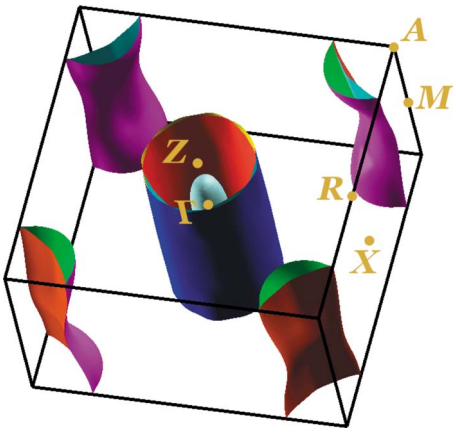

FIG. 6. (Color online) The calculated Fermi surface of $FeTe_{0.66}Se_{0.34}$.

effect upon electronic structures was studied by using virtual crystal calculations.

Figure 5 displays the calculated band structure; there are indeed three bands near Γ and two bands near M that cross the Fermi energy. In particular, the innermost band near Γ does show significant dispersion along the Γ-Z direction. As a result, our calculations give five Fermi surfaces as shown in Fig. 6. The calculated band structure to a large extent resembles those of the iron-arsenide superconductors.

Qualitatively, the calculated Fermi surfaces agree well with our experiments. However, there are some important quantitative discrepancies. Figure 7 illustrates the measured band structure along Γ-M as reproduced from Fig. 2(c), together with the calculated bands. One finds that the size of the calculated γ Fermi surface is much smaller than the measured one. However, the calculated α, β, and γ bands match the data after scaled by 3.125 and shifted down by 45 meV, except the Fermi crossings of the measured and calculated γ band are different. The scaling factor illustrates the correlation effects in this material. The experimental Fermi velocity

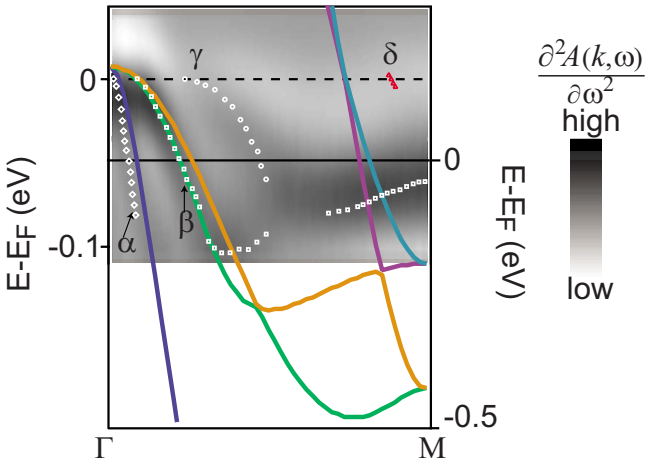

FIG. 7. (Color online) Comparison of the band structure of the ARPES data and the DFT calculation results along the Γ-M cut. Note: the energy scale of the calculated band structure at the right side is 3.125 times of the energy scale of the experimental data at the left side.

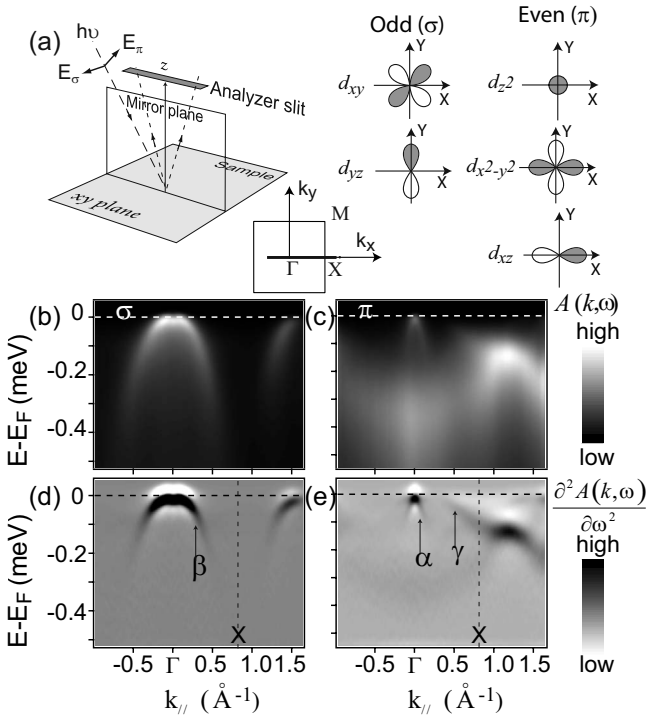

FIG. 8. (a) Cartoon of the polarization dependence experiment, and the symmetry of the orbitals with respect to the mirror plane defined by sample normal and Γ-*X*. (b) The photoemission intensity along the Γ-*X* direction measured at the σ geometry and (d) its second derivative with respect to energy. (c) The photoemission intensity along the Γ-*X* direction measured at the π geometry and (e) its second derivative. Data were taken with 100 eV photons at SLS, and the temperature was 10 K.

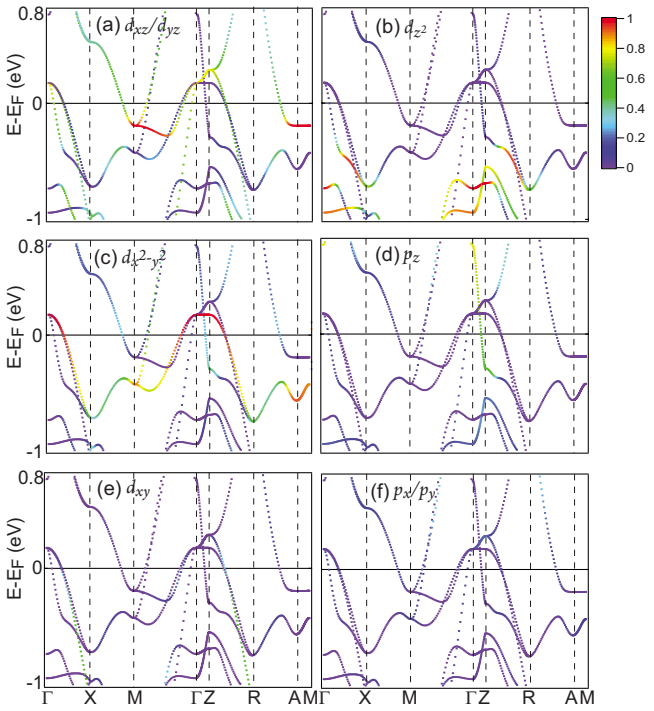

FIG. 9. (Color online) Contributions of various Fe 3*d* and Te/Se *p* orbitals to the calculated band structure of $FeTe_{0.66}Se_{0.34}$.

of α, β, and γ bands are 0.62, 0.4, and 0.137 eV Å, respectively. On the other hand, the measured Fermi surface around *M* is much smaller than the calculated ones. Similar to the iron-pnictides,[27] the renormalization factors of the bands vary in different regions of the Brillouin zone.

We note that in order to obtain accurate band renormalization factors, it is crucial to compare the data with the calculation conducted *for the same Se doping*. We have calculated the band structures of $FeTe_{1-x}Se_x$ with a series of doping, and found that the band structure around Γ evolves rapidly with increasing Se concentration. Similar conclusion can be drawn from the published FeSe and FeTe band structures by Subedi *et al.*[28]

V. POLARIZATION DEPENDENCE

For a multiband and multiorbital superconductor, it is crucial to understand the orbital characters of the band structure near E_F. In photoemission, such information can be obtained to a large extent in the polarization dependence. Figure 8(a) illustrates two types of experimental setup with linearly polarized light. The incident beam and the sample surface normal define a mirror plane. For the π (or σ) experimental geometry, the electric field direction ($\hat{\varepsilon}$) of the incident photons is in (or out of) the mirror plane. The matrix element of the photoemission process can be described by

$$|M_{f,i}^{\mathbf{k}}| \propto |\langle \phi_f^{\mathbf{k}} | \hat{\varepsilon} \cdot \mathbf{r} | \phi_i^{\mathbf{k}} \rangle|^2,$$

where $\phi_i^{\mathbf{k}}$ and $\phi_f^{\mathbf{k}}$ are the initial- and final-state wave functions, respectively.[29] In our experimental setup, the momentum of the final-state photoelectron is in the mirror plane and $\phi_f^{\mathbf{k}}$ can be approximated by a plane wave. Therefore, $\phi_f^{\mathbf{k}}$ is always even with respect to the mirror plane. In the π geometry, $(\hat{\varepsilon} \cdot \mathbf{r})$ is even, to give a finite photoemission matrix element, $|\phi_i^{\mathbf{k}}\rangle$ must be even with respect to the mirror plane. Thus only even state is probed in the π experimental geometry. On the other hand, one could similarly deduce that only odd state is observed in the σ geometry.

In contrast to the data measured with circularly polarized light in Figs. 2(i) and 2(j), only the β band is observed in the σ geometry [Figs. 8(b) and 8(d)], while just the α and γ bands are observed in the π geometry [Figs. 8(c) and 8(e)]. Based on the symmetry of different orbitals illustrated in Fig. 8(a), the β band is odd with respect to the mirror plane, while the α and γ bands are even along the Γ-*X* direction. Therefore, the β band has to be made of d_{xy} and/or d_{yz} orbitals, while the α and γ bands may be consisted of $d_{x^2-y^2}$, d_{z^2}, and/or d_{xz}.

These experimental findings of the symmetry properties of the band structure are well captured by the band structure calculation. In Fig. 9, the orbital characters of the bands are shown by the false color plot. Near the Fermi energy, the α band is mainly consisted of d_{xz}/d_{yz} orbitals, which should be purely d_{xz} along the Γ-*X* direction. The β band is consisted of mainly d_{xz} and d_{yz} orbitals, and some d_{xy} orbitals; while the γ band is consisted of $d_{x^2-y^2}$ orbital. Along the Γ-*Z* direction, the band structure near E_F has some contributions from the p_z orbital and small contributions from the d_{z^2} or-

TABLE I. The contributions of Fe $3d$ and Te/Se p orbitals to the bands in $FeTe_{0.66}Se_{0.34}$ near E_F along the $\Gamma - X$ direction.

	d_{z^2}	d_{xz}	d_{yz}	$d_{x^2-y^2}$	d_{xy}	p_z	p_x+p_y
α	0.0391	0.6702	0	0.0182	0	0.0791	0.0767
β	0	0	0.6579	0	0.2359	0	0.0463
γ	0.0033	0.0434	0	0.9391	0	−0.0001	0.0069

bital. They all have even symmetry and thus can be observed in the π experimental geometry. The small ellipsoidal Fermi surface near zone center is mainly contributed by the d_{z^2} orbital for FeAs-based compounds, while for $FeTe_{0.66}Se_{0.34}$, Te/Se p_z orbital plays an important role. To have a more quantitative picture, we have listed the contributions of various orbitals to the states at E_F in Table I, which are the coefficients of the calculated corresponding Bloch wave functions projected into the orbitals.

VI. DISCUSSION

Although the chalcogen ions contribute little spectral to the density of states (DOS) near the Fermi energy, the Fe $3d$ related band structure in iron chalcogenides does show significant difference compared with that of iron pnictides. Recently, it is even proposed that the polarization of the As p orbitals might be the cause of the unconventional superconductivity in FeAs-based superconductors.[11] Therefore in this regard, the electronic consequences related to the chalcogen or pnicogen anions in the iron-based superconductors are particularly interesting to explore.

In general, $Fe_{1.04}Te_{0.66}Se_{0.34}$ has similar Fermi surface and band structure as the iron-pnictides.[22,30] However, there are some important differences. For example, the three bands near Γ are well separated in this iron chalcogenides, each with distinct symmetry. On the other hand in recent polarization dependence studies of the $BaFe_{1.82}Co_{0.18}As_2$, only two features around Γ were observed.[22] Moreover, the inner feature is a mixture of orbitals of both even and odd symmetries, while the outer feature is even in symmetry. Moreover, our calculations show that the Te $5p$ orbitals contribute to the density of states near the Fermi energy, while Fe $3d_{z^2}$ orbital contributes very little in this iron chalcogenide. Furthermore, there is a small ellipsoidal Fermi surface near the zone center of $Fe_{1.04}Te_{0.66}Se_{0.34}$, while for iron pnictides such a small Fermi pocket has not been unambiguously observed in the paramagnetic normal state.

Compared with the electronic structure of $Fe_{1+y}Te$ obtained earlier,[31] the $Fe_{1.04}Te_{0.66}Se_{0.34}$ electronic structure behaves differently in the following two aspects. First, three bands, α, β, and γ, are clearly observed around Γ for $Fe_{1.04}Te_{0.66}Se_{0.34}$, whereas only two bands were distinguished in $Fe_{1+y}Te$. Second, a weak Fermi surface was observed around X in $Fe_{1+y}Te$, which was argued to be a folded Fermi surface by the spin density wave. For $Fe_{1.04}Te_{0.66}Se_{0.34}$, neutron-scattering experiments have found incommensurate short-range magnetic order below 50 K (Ref. 12); however, our measurements with two different photon polarizations confirm the absence of states near E_F around X. Furthermore, no band splitting that is associated with the SDW in $BaFe_2As_2$ and $SrFe_2As_2$ is observed here. This might suggest that such a short-range magnetic order should be very weak in $Fe_{1.04}Te_{0.66}Se_{0.34}$.

VII. CONCLUSION

To summarize, we have studied the electronic structure of $Fe_{1.04}Te_{0.66}Se_{0.34}$. Both the ARPES and DFT calculations reveal one inner closed Fermi pocket and two outer cylindrical Fermi surfaces near Γ, and two electronlike Fermi surfaces near the M point. There are no states near the Fermi energy around the X point. Polarization dependence measurements further elucidate the symmetry of the band structure. The ARPES results qualitatively agree with the DFT calculations. Compared with the iron pnictides, although many aspects of the band structures are similar, there are also significant differences, particularly in their electronic structures near Γ at the paramagnetic normal state. Our results provide a comprehensive picture on the electronic structure of $Fe_{1.04}Te_{0.66}Se_{0.34}$ and shed light on the role of anions in iron-based superconductors.

ACKNOWLEDGMENTS

Part of this work was performed at the Surface and Interface Spectroscopy beamline, Swiss Light Source, Paul Scherrer Institute, Villigen, Switzerland. We thank C. Hess and F. Dubi for technical support. This work was supported by the NSFC, MOE, MOST (National Basic Research Program No. 2006CB921300), and STCSM of China.

*dlfeng@fudan.edu.cn

[1] Y. Kamihara, T. Watanabe, M. Hirano, and H. Hosono, J. Am. Chem. Soc. **130**, 3296 (2008).

[2] X. H. Chen, T. Wu, G. Wu, R. H. Liu, H. Chen, and D. F. Fang, Nature (London) **453**, 761 (2008).

[3] Z. A. Ren *et al.*, Chin. Phys. Lett. **25**, 2215 (2008).

[4] M. Rotter, M. Tegel, D. Johrendt, I. Schellenberg, W. Hermes, and R. Pottgen, Phys. Rev. B **78**, 020503(R) (2008).

[5] M. Rotter, M. Tegel, and D. Johrendt, Phys. Rev. Lett. **101**, 107006 (2008).
[6] M. J. Pitcher, D. R. Parker, P. Adamson, S. J. C. Herkelrath, A. T. Boothroyd, R. M. Ibberson, M. Brunellid, and S. J. Clarke, Chem. Commun. **2008**, 5918.
[7] J. H. Tapp, Z. Tang, B. Lv, K. Sasmal, B. Lorenz, P. C. W. Chu, and A. M. Guloy, Phys. Rev. B **78**, 060505(R) (2008).
[8] F. C. Hsu, J. Luo, K. Yeh, T. Chen, T. Huang, P. Wu, Y. Lee, Y. Huang, Y. Chu, D. Yan, and M. Wu, Proc. Natl. Acad. Sci. U.S.A. **105**, 14262 (2008).
[9] K. W. Yeh, T. Huang, Y. Huang, T. Chen, F. Hsu, P. Wu, Y. Lee, Y. Chu, C. Chen, J. Luo, D. Yan, and M. Wu, Europhys. Lett. **84**, 37002 (2008).
[10] S. Margadonna, Y. Takabayashi, Y. Ohishi, Y. Mizuguchi, Y. Takano, T. Kagayama, T. Nakagawa, M. Takata, and K. Prassides, Phys. Rev. B **80**, 064506 (2009).
[11] G. A. Sawatzky, I. Elfimov, J. Vandenbrink, and J. Zaanen, Europhys. Lett. **86**, 17006 (2009).
[12] W. Bao *et al.*, Phys. Rev. Lett. **102**, 247001 (2009).
[13] S. L. Li *et al.*, Phys. Rev. B **79**, 054503 (2009).
[14] F. Ma, Z.-Y. Lu, and T. Xiang, Phys. Rev. B **78**, 224517 (2008).
[15] C. Fang, H. Yao, W. F. Tsai, J. P. Hu, and S. A. Kivelson, Phys. Rev. B **77**, 224509 (2008).
[16] J. Dai, Q. Si, J.-X. Zhu, and E. Abrahams, Proc. Natl. Acad. Sci. U.S.A. **106**, 4118 (2009).
[17] F. Ma, W. Ji, J. Hu, Z. Y. Lu, and T. Xiang, Phys. Rev. Lett. **102**, 177003 (2009).
[18] C. Fang, B. A. Bernevig, and J. Hu, Europhys. Lett. **86**, 67005 (2009).
[19] Cenke Xu and Jiangping Hu, arXiv:0903.4477 (unpublished).
[20] J. Dong *et al.*, Europhys. Lett. **83**, 27006 (2008).
[21] K. Nakayama, T. Sato, P. Richard, T. Kawahara, Y. Sekiba, T. Qian, G. Chen, J. Luo, N. Wang, H. Ding, and T. Takahashi, arXiv:0907.0763 (unpublished).
[22] Y. Zhang, B. Zhou, F. Chen, J. Wei, M. Xu, L. Yang, C. Fang, W. Tsai, G. Cao, Z. Xu, M. Arita, C. Hong, K. Shimada, H. Namatame, M. Taniguchi, J. Hu, and D. Feng, arXiv:0904.4022 (unpublished).
[23] L. X. Yang *et al.*, Phys. Rev. Lett. **102**, 107002 (2009).
[24] P. Giannozzi *et al.*, http://www.quantum-espresso.org.
[25] J. P. Perdew, K. Burke, and M. Ernzerhof, Phys. Rev. Lett. **77**, 3865 (1996).
[26] D. Vanderbilt, Phys. Rev. B **41**, 7892 (1990).
[27] D. H. Lu *et al.*, Nature (London) **455**, 81 (2008).
[28] A. Subedi, L. Zhang, D. J. Singh, and M. H. Du, Phys. Rev. B **78**, 134514 (2008).
[29] A. Damascelli, Z. Hussain, and Z.-X. Shen, Rev. Mod. Phys. **75**, 473 (2003).
[30] Y. Zhang *et al.*, Phys. Rev. Lett. **102**, 127003 (2009).
[31] Y. Xia, D. Qian, L. Wray, D. Hsieh, G. F. Chen, J. L. Luo, N. L. Wang, and M. Z. Hasan, Phys. Rev. Lett. **103**, 037002 (2009).